Cation-chloride cotransporters and the polarity of GABA signaling in mouse hippocampal parvalbumin interneurons

Yo Otsu[1,2,3,4], Florian Donneger[1,2,3], Eric J Schwartz[1,2,3] and Jean Christophe Poncer[1,2,3*]

[1] Inserm UMR-S 1270, 75005 Paris, France.; [2] Sorbonne Université, F75005, Paris, France ;

[3] Institut du Fer à Moulin, F75005, Paris, France.

[4] Present address: Pain Management Research Institute, Kolling Institute of Medical Research, Northern Clinical School, The University of Sydney and Royal North Shore Hospital, St. Leonards, New South Wales, Australia

Running title: GABA signaling in hippocampal parvalbumin interneurons

Keywords: synaptic transmission, GABA, KCC2, chloride, transporters, hippocampus

Category: Research paper

* Correspondence should be addressed to Jean Christophe Poncer:

INSERM UMR-S 1270

17 rue du Fer à Moulin

75005 Paris, France

Tel. +33 1 45 87 61 18

E-mail : jean-christophe.poncer@inserm.fr

Key point summary

- Cation-chloride cotransporters (CCCs) play a critical role in controlling the efficacy and polarity of GABAA receptor (GABAAR)-mediated transmission in the brain, yet their expression and function in GABAergic interneurons has been overlooked.
- We compared the polarity of GABA signaling and the function of CCCs in mouse hippocampal pyramidal neurons and parvalbumin-expressing interneurons.
- Under resting conditions, GABAAR activation was mostly depolarizing and yet inhibitory in both cell types. KCC2 blockade further depolarized the reversal potential of GABAAR-mediated currents often above action potential threshold.
- However, during repetitive GABAAR activation, the postsynaptic response declined independently of the ion flux direction or KCC2 function, suggesting intracellular chloride buildup is not responsible for this form of plasticity.
- Our data demonstrate similar mechanisms of chloride regulation in mouse hippocampal pyramidal neurons and parvalbumin interneurons.

Abstract

Transmembrane chloride gradients govern the efficacy and polarity of GABA signaling in neurons and are usually maintained by the activity of cation chloride cotransporters, such as KCC2 and NKCC1. Whereas their role is well established in cortical principal neurons, it remains poorly documented in GABAergic interneurons. We used complementary electrophysiological approaches to compare the effects of GABAAR activation in adult mouse hippocampal parvalbumin interneurons (PV INs) and pyramidal cells (PCs). Loose cell attached, tight-seal and gramicidin-perforated patch recordings all show GABAAR-mediated transmission is slightly depolarizing and yet inhibitory in both PV INs and PCs. Focal GABA uncaging in whole-cell recordings reveal that KCC2 and NKCC1 are functional in both PV INs and PCs but differentially contribute to transmembrane chloride gradients in their soma and dendrites. Blocking KCC2 function depolarizes the reversal potential of GABAAR-mediated currents in PV INs and PCs, often beyond firing threshold, showing KCC2 is essential to maintain the inhibitory effect of GABAARs. Finally, we show that repetitive 10 Hz activation of GABAARs in both PV INs and PCs leads to a progressive decline of the postsynaptic response independently of the ion flux direction or KCC2 function. This suggests intraneuronal chloride buildup may not predominantly contribute to activity-dependent plasticity of GABAergic synapses in this frequency range. Altogether our data demonstrate similar mechanisms of chloride regulation in mouse hippocampal PV INs and PCs and suggest KCC2 downregulation in the pathology may affect the valence of GABA signaling in both cell types.

Introduction

Information representation and processing in the cerebral cortex relies on the dynamic interaction between ensembles of glutamatergic principal neurons and local, highly diversified GABAergic interneurons (Buzsaki, 2010). These interneurons mediate feedforward and/or feedback inhibition onto principal cells (PCs) and thereby control their coordinated activity (Klausberger & Somogyi, 2008). In particular, parvalbumin-expressing interneurons (PV INs), which receive excitatory inputs from both local and distant PCs, in turn provide them with fast perisomatic inhibition (Hu *et al.*, 2014). Fast inhibitory signaling by PV INs controls the timing of principal cell activity (Pouille & Scanziani, 2001) and plays a major role in the generation of rhythmic activities (Klausberger & Somogyi, 2008; Amilhon *et al.*, 2015; Gan *et al.*, 2017) as well as the segregation of PCs into functional assemblies (Agetsuma *et al.*, 2018). However, in addition to excitatory inputs from PCs, PV INs also receive GABAergic innervation from local interneurons (Chamberland & Topolnik, 2012), including some specialized in interneuron inhibition (Gulyas *et al.*, 1996), as well as long-range projecting interneurons (Freund & Antal, 1988). Although GABAergic synapses formed onto PV INs share many properties with those impinging onto principal cells, input- and cell-specific properties were also reported (Chamberland & Topolnik, 2012). For instance, predominant expression of the α1 GABAAR subunit confers PV INs with faster postsynaptic current kinetics as compared to PCs (Gao & Fritschy, 1994; Bartos *et al.*, 2002).

Since GABAARs are predominantly chloride-permeable channels (Bormann *et al.*, 1987), transmembrane chloride gradients also represent a major source of variability for GABA signaling. Cation chloride cotransporters (CCCs) play a critical role in regulating chloride

gradients in neurons. Thus, the Na^+ K^+ Cl^- transporter NKCC1 and the K^+ Cl^- transporter KCC2 are secondary active transporters that regulate intraneuronal chloride using the Na^+ and K^+ electrochemical gradients generated by the Na/K-ATPase (Blaesse *et al.*, 2009). Delayed, postnatal KCC2 expression has been shown to contribute to a progressive shift in intraneuronal chloride and the polarity of GABA signaling in cortical PCs *in vitro* (Rivera *et al.*, 1999). *In vivo*, GABA was shown to depolarize immature PCs and yet exert a predominantly inhibitory action on their activity (Kirmse *et al.*, 2015), due to membrane resistance shunting.

However, much less is known regarding chloride handling in GABAergic interneurons. Thus, the reversal potential of GABAAR-mediated currents (E_{GABA}) was suggested to be more depolarized in unidentified hippocampal *stratum radiatum* interneurons compared with neighboring PCs (Patenaude *et al.*, 2005). In addition, the driving force of GABAAR-mediated currents was shown to remain unchanged during postnatal maturation, in *stratum oriens* interneurons (Banke & McBain, 2006) but appear to exhibit a hyperpolarizing shift in dentate gyrus basket cells (Sauer & Bartos, 2010). Although most interneurons subtypes were shown to strongly express KCC2 in the adult rat hippocampus (Gulyas *et al.*, 2001), how CCC expression or function control the polarity and efficacy of GABA signaling in these cells remains unknown. One difficulty in addressing this question relates to the diversity and bias of experimental approaches used to evaluate the effect of GABA or chloride transport with minimal perturbation of the neuronal integrity. Here, we used a combination of both invasive and non-invasive *in vitro* electrophysiological approaches to compare GABA signaling in mouse CA1 PV INs and PCs in adult mouse hippocampus. Our results reveal that

GABA predominantly exerts depolarizing yet inhibitory actions over both cell types. KCC2 and NKCC1 appear to be functional in both PV INs and PCs even though the two cell types exhibit different somato-dendritic chloride gradients. Finally, we demonstrate that CCCs do not contribute in activity-dependent depression of GABAAR-mediated transmission upon moderate activation frequency (10 Hz). Together our results demonstrate that, in the adult hippocampus, PV INs and PCs both rely on CCC activity to maintain inhibitory GABA signaling.

Methods

Animals

Pvalb$^{tm1(cre)Arbr}$/J mice were crossed with *Gt(ROSA)26Sor*$^{tm14(CAG-tdTomato)Hze}$/J (Ai14) reporter mice expressing the red fluorescent protein tdTomato. The genetic background of both *Pvalb*$^{tm1(cre)Arbr}$/J and Ai14 mice was C57BL/6J and dual homozygous male or female mice typically aged 35-70 days were used in all experiments. Since we did not observe sex-dependent differences in the biological parameters tested in this study, data from animals of either sex were grouped. All procedures conformed to the International Guidelines on the ethical use of animals, the French Agriculture and Forestry Ministry guidelines for handling animals (decree 87849, licence A 75-05-22) and were approved by the Charles Darwin ethical committee (APAFIS#4018-2015111011588776 v7).

Immunohistochemistry and imaging

Mice were deeply anesthetized by intraperitoneal injection of ketamine/xylazine (100/20 $mg.kg^{-1}$) and perfused transcardially with oxygenated ice-cold solution containing in mM : 110 choline-Cl, 2.5 KCl, 1.25 NaH_2PO_4, 25 $NaHCO_3$, 25 glucose, 0.5 $CaCl_2$, 7 $MgCl_2$, 11.6 ascorbic acid, 3.1 Na pyruvate (~300 mOsm), equilibrated with 95% O_2-5% CO_2. Brains were removed and fixed for 4-5 h at 4°C with 4% paraformaldehyde in 0.1M sodium phosphate buffer (pH 7.5) and cryoprotected in 30% sucrose in PBS for an additional 24h. Coronal, 40 µm-thick sections were cut with a cryotome. Free-floating sections were rinsed in PBS and incubated for 4 h in PBS supplemented with 0.5% Triton X-100 and 5% normal goat serum. They were then incubated for 48 h at 4°C with rabbit polyclonal KCC2 antibody (1:400) diluted in PBS supplemented with 0.1% Triton X-100 and 5% normal goat serum before being

rinsed in PBS and incubated overnight at 4°C with biotinylated WFA lectin (1:500). The sections were then rinsed in PBS and then incubated for 4h with donkey anti-rabbit Cy5, rinsed in PB and incubated for 40 min with streptavidin Alexa-488. After rinsing in PB, the sections were mounted with Mowiol/Dabco (25 $mg.ml^{-1}$) and stored at 4°C.

KCC2-immunolabeled sections were imaged with a Leica SP5 confocal microscope using a 63x 1.40-N.A. objective with 2X electronic magnification and Ar/Kr laser set at 488, 561 and 633 nm for excitation of Alexa-488, td-tomato and Cy5, respectively. Stacks of 10 optical sections were acquired at a pixel resolution of 0.12 µm and a z-step of 0.29 µm.

Electrophysiological recordings

Mice were deeply anesthetized by intraperitoneal injection of ketamine/xylazine (100/20 $mg.kg^{-1}$, Sigma-Aldrich) and transcardially perfused with ice-cold solution containing (in mM): 110 choline-Cl, 2.5 KCl, 1.25 NaH_2PO_4, 25 $NaHCO_3$, 25 glucose, 0.5 $CaCl_2$, 7 $MgCl_2$, 11.6 ascorbic acid, 3.1 Na pyruvate (~300 mOsm), equilibrated with 95% O_2-5% CO_2. Mice were then decapitated and 350 µm-thick parasagittal brain slices were prepared with a vibratome (Microm, Thermo Scientific, France) in the same ice-cold solution and maintained in a humidified interface chamber saturated with 95% O_2-5% CO_2 for 10 minutes at 34°C and then at room temperature until use. Artificial cerebrospinal fluid (ACSF) for slice maintenance and recording contained (in mM): 126 NaCl, 26 $NaHCO_3$, 10 D-glucose, 3.5 KCl, 1.6 $CaCl_2$, 1.2 $MgCl_2$, 1.25 NaH_2PO_4. For recordings, slices were transferred into a chamber

158 (BadController V; Luigs & Neumann) maintained at 32°C and mounted on an upright
159 microscope (BX51WI; Olympus). Slices were superfused with ACSF at a rate of 2.5 ml.min^{-1}.

160 Loose cell-attached recordings (seal resistance: 15-25 MΩ) were made using 4-6 MΩ
161 borosilicate glass pipettes containing normal ACSF or HEPES-buffered saline containing (in
162 mM): 150 NaCl, 3.5 KCl, 1.6 $CaCl_2$, 1.2 $MgCl_2$, 10 HEPES, pH 7.4 with NaOH (300 mOsm) in the
163 presence of excitatory transmission blockers (10 µM NBQX and 50 µM D-APV) at a holding
164 potential of 0 mV. Recordings were established by gently pushing the pipette against the
165 membrane of the cell. Signals were filtered at 4 kHz and acquired using pClamp software
166 (Molecular Devices) in voltage clamp mode at a sampling rate of 10-20 kHz.

167

168 Tight cell-attached recordings (Perkins, 2006) were performed in the presence of 10 µM
169 NBQX and 50 µM D-APV under current-clamp configuration (I=0 mode) to evaluate the
170 polarity of GABAAR-mediated potentials. Recording pipettes (4-9 MΩ) were filled with the
171 HEPES-buffered saline. Seal resistance in the cell-attached mode was >4 GΩ. Voltage signals
172 were filtered at 4 kHz and sampled at 10-20 kHz.

173

174 For whole-cell recordings, pipettes (3–5 MΩ resistance) were filled with a solution containing
175 (in mM): 115 K-gluconate, 25.4 KCl, 10 HEPES, 10 EGTA, 1.8 $MgCl_2$, 2 Mg-ATP, 0.4 Na_3-GTP,
176 pH 7.4 (290 mOsm) supplemented with Alexa 594 (20 µM) to check cell morphology. Images
177 of the soma and dendrites were acquired at least 15 min after break in, using 535 nm
178 excitation light (CoolLED) to prevent RuBi-GABA uncaging. Cells were voltage-clamped at -60
179 or -70 mV. Voltage was corrected *post hoc* for liquid junction potential (-11 mV) and voltage

drop across the series resistance (<25 MΩ) of the pipette. Currents were filtered at 4 kHz and sampled at 10 kHz.

For gramicidin-perforated patch recordings, the tip of the recording pipette was filled with gramicidin-free solution containing (in mM): 120 KCl, 10 HEPES, 11 EGTA, 1 $CaCl_2$, 2 $MgCl_2$, 35 KOH, 30 glucose adjusted to pH 7.3 with KOH (300 mOsm). The pipette was then backfilled with the same solution containing 100 µg/ml gramicidin and 20 µM Alexa 488 to verify membrane integrity during the recording. Gramicidin was prepared as a stock solution at 50 mg/ml in DMSO. Pipette resistance was 4-5 MΩ. Cells were voltage-clamped at -70 mV. Recordings were started once series resistance was less than 100 MΩ (52.5±7.6 MΩ for PV INs (n=10) and 69.1±5.8 MΩ for PCs (n=16)). The Donnan potential between the pipette solution and cell cytoplasm was measured (Kim & Trussell, 2007) after spontaneous membrane rupture (11.7±1.1 mV; n = 4). The Donnan potential was partly offset by a liquid junction potential of -4 mV. Therefore, the holding potential in gramicidin-perforated recordings reads 7.7 mV more hyperpolarized than the actual membrane potential. Potentials were corrected for this residual potential and voltage drop across the series resistance of the pipette. Spontaneous action potentials (APs) and resting membrane potential (Vm) were monitored under current clamp configuration (I=0 mode) while E_{GABA} was measured by RuBi-GABA photolysis under voltage clamp. Vm was estimated by averaging membrane potential every 500 ms for 30-60 sec in normal ACSF. Membrane potential in the presence of drugs for photolysis were similarly computed over 30-60 sec (Fig. 6A). The threshold for action potential initiation was determined from the first peak in the third derivative of action potential waveforms averaged from > 4 APs (Henze & Buzsaki, 2001). Currents were filtered at 10 kHz and sampled at 10-20 kHz.

203

204 *Photolysis*

205 Photolysis of RuBi-GABA (15 µM) onto parvalbumin positive interneurons (PV INs) or
206 pyramidal cells (PCs) was performed in the presence of 10 µM NBQX, 50 µM D-APV, 2 µM
207 CGP55845 and 1 µM tetrodotoxin (TTX). A 405 nm laser diode beam (Deepstar, Omicron,
208 Photon Lines, France) conducted through a multimode optic fibre and alignment device
209 (Prairie Technologies, Middleton, WI, USA) was set to generate a 3-5 µm spot in the
210 objective focus and directed to the soma or distal dendrites of the recorded neurons. The
211 power of the laser head output was controlled using Omicron Laser Controller v2.97, while
212 trigger and pulse duration were set using pClamp software and a Digidata controller.
213 Photolysis was induced by a 0.5-1 msec pulse at 10 mW on the soma or 3-5 msec at 10 mW
214 on distal dendrites. Series of 15 s voltage steps with a 5 mV increment were applied to the
215 pipette with an inter-episode interval of 40 sec. Laser pulses were delivered at 12 sec after
216 the onset of the voltage step to allow for stabilization of the holding current. The amplitude
217 of GABA-evoked currents was computed as the difference between the current measured
218 over a 4 ms window centered on the peak and the baseline current averaged over 3 ms prior
219 to the laser flash. The distance from soma for dendritic uncaging was measured offline with
220 NeuronJ (Meijering *et al.*, 2004), based on Alexa 594 fluorescence imaging of the recorded
221 neuron.

222

223 *Drug application*

224 Isoguvacine (100 µM; Tocris Bioscience) was dissolved in normal ACSF supplemented with 2
225 µM Alexa 488 to detect regions puffed through a patch pipette using a Picosplitzer III (5 sec

at 10 psi). All other drugs were bath applied: NBQX, D-AP5, were from Hello Bio (Bristol, UK). Isoguvacine, RuBi-GABA trimethylphosphine, CGP55845, VU0463271 were from Tocris Bioscience (Bristol, UK). TTX was from Latoxan. All other drugs were from Sigma-Aldrich France. CGP55845, VU0463271 and bumetanide were dissolved in DMSO for stock solutions.

Data analysis

Electrophysiological data analysis was performed offline using Clampfit 10 (Molecular Devices, USA) and custom routines written in Igor Pro 6 (WaveMetrics, USA).

Statistical analysis

The results are presented as mean ± SEM throughout the manuscript and in all figures. For statistical analyses, non-parametric Mann-Whitney or Wilcoxon signed-rank tests were used unless Shapiro-Wilk normality test was passed and Student's t-test could be used. Multiple linear regression analysis was performed using SigmaPlot 12,5 (SPSS). Statistical significance was set at $p<0.05$.

Results

KCC2 expression in hippocampal parvalbumin interneurons

Although the expression and function of CCCs are well characterized in hippocampal principal neurons, whether they are expressed and functional in GABAergic interneurons remains largely unexplored. We used immunohistochemistry in *Pvalb*$^{tm1(cre)Arbr/J}$*::Ai14* mice to investigate KCC2 expression in mouse hippocampal parvalbumin interneurons (PV INs) (Le Roux *et al.*, 2013).

In all hippocampal subfields, KCC2 expression was observed in td-tomato-positive interneurons (Figure 1A). As in PCs, KCC2 immunostaining in PV INs was mostly pericellular, likely reflecting predominant membrane expression (Figure 1B). However, KCC2 expression in PV INs was sometimes difficult to distinguish from that in neighboring PCs. To circumvent this problem, we used extracellular matrix staining to precisely visualize PV IN contours. Hippocampal PV INs somata and proximal dendrites are wrapped by a chondroitin sulfate proteoglycan-rich extracellular matrix, called perineuronal net (PNN) (Hartig *et al.*, 1992). Thus using specific staining of PNNs with Wisteria Floribunda Agglutinin (WFA), KCC2 immunostaining in PV INs could be distinguished from that in adjacent principal neurons as it was surrounded by WFA staining, further confirming KCC2 expression in PV INs (Figure 1B).

These results support the conclusion that KCC2 protein is expressed at the membrane of PV INs in the adult mouse hippocampus.

(Figure 1 near here)

Net effect of GABAAR activation on CA1 pyramidal neurons and parvalbumin interneurons.

We next asked whether cation-chloride cotransporters are functional in CA1 PV INs and how they influence GABAAR-mediated signaling in these cells. Loose cell-attached recordings allow detection of action potentials from identified neurons with minimal perturbation of their physiology (Llano & Marty, 1995). We first used this approach to evaluate the excitatory *vs.* inhibitory nature of GABA transmission in CA1 PV INs and neighboring pyramidal neurons (PCs). The effect of GABAAR activation was tested by locally puffing the GABAAR agonist isoguvacin (100 µM, 5 s) onto the soma of the recorded cell. In order to prevent the influence of polysynaptic EPSPs, recordings were performed in the presence of AMPA and NMDA receptor antagonists. Under these conditions however only a few (5 of 27) PV INs exhibited spontaneous firing (Figure 2A). Out of 27 recorded PV INs, isoguvacine induced firing in 1, blocked firing in 5 and had no detectable effect in 21 interneurons. In the presence of the NKCC1 antagonist bumetanide (10 µM), however, isoguvacine suppressed firing in 7 of 14 PV INs, suggesting bumetanide hyperpolarizes E_{GABA} in PV INs. The KCC2 specific antagonist VU0463271 (10 µM), on the other hand, increased the proportion of PV INs that were excited by isoguvacine (3 of 13 cells) while the proportion of cells that were inhibited was similar to that observed in the presence of bumetanide (6 of 13 cells; Figure 2C). These results suggest the effect of GABAA receptor activation is predominantly inhibitory in PV INs and is influenced by the function of both KCC2 and NKCC1.

(figure 2 near here)

In neighboring PCs, isoguvacine had little effect on firing (5 of 23 cells), mostly owing to the fact that most of them were silent (18 of 23 cells) prior to isoguvacine application, making it difficult to assess the inhibitory or excitatory nature of GABA signaling. Bumetanide had only very little effect on the proportion of pyramidal cells excited (1 of 10 cells) or inhibited (1 of

10 cells) by isoguvacine, whereas VU0463271 induced a large increase in the proportion of excited neurons (7 of 11 cells) (Figure 2D). This excitatory effect was still observed in the presence of both bumetanide and VU0463271 (3 of 11 cells), as with PV INs. In slices from younger (3-7 days old) animals, however, isoguvacine application was sufficient to trigger firing in 26 out of 66 neurons under control conditions, suggesting GABA signaling in PCs was clearly excitatory at this age.

Altogether, these results suggest KCC2 and NKCC1 are functional in both CA1 pyramidal cells and PV INs and influence the efficacy of GABA signaling. However, the high proportion of silent neurons under our recording conditions makes it difficult to draw firm conclusions regarding the polarity of GABA transmission in these cells under physiological conditions.

Tight-seal, cell-attached recordings provide another, minimally invasive approach to detect the polarity of synaptic potentials without rupturing the cell membrane and perturbing transmembrane ionic gradients (Perkins, 2006). In particular, gigaseal recordings allow a fairly reliable measurement of both neuronal resting membrane potential and the polarity (but not the actual amplitude) of synaptic potentials (Mason *et al.*, 2005; Perkins, 2006). We recorded currents evoked by GABAAR activation with isoguvacine in gigaseal mode from both CA1 PV INs and PCs (Figure 3A). In both cell types, isoguvacine-induced potentials were predominantly depolarizing (5 of 7 and 5 of 6 cells, respectively). This proportion was similar to recordings from immature (P3-P7) CA1 pyramidal neurons (6 of 9 cells, Figure 3B). Together, these results suggest that, at least in the absence of glutamatergic drive, both CA1 PCs and PV INs are predominantly depolarized upon GABAAR activation, even though a

315 significant fraction are functionally inhibited, likely due to shunting of their membrane
316 resistance (Staley & Mody, 1992).

317 (Figure 3 near here)

318 **KCC2-mediated chloride extrusion in CA1 parvalbumin interneurons**

319 Transmembrane chloride transport can be directly estimated from whole-cell recordings of
320 GABA-evoked currents while clamping somatic chloride concentration (Khirug *et al.*, 2008;
321 Gauvain *et al.*, 2011). The gradient of the reversal potential of GABAAR-mediated currents
322 (E_{GABA}) along the somato-dendritic membrane then reflects actual transmembrane chloride
323 extrusion. We compared E_{GABA} gradients in CA1 PV INs and PCs using local photolysis of
324 RubiGABA (15 µM, 0.5-5 ms laser pulse, see Methods). As in other cortical neurons (Khirug *et*
325 *al.*, 2008; Gauvain *et al.*, 2011), E_{GABA} in PV INs, was always more depolarized for somatically-
326 evoked currents, as compared to currents evoked onto dendrites 50-250 µm away from the
327 soma (Figure 4). This somato -dendritic gradient (ΔE_{GABA}) however was significantly steeper
328 in neighboring PCs as compared with PV INs (-21.1 ± 1.7 *vs* -12.6 ± 0.7 mV/100 µm; 11
329 dendritic sites in 8 cells and 17 dendritic sites in 9 cells, respectively, $p<0.001$; Figure 5A-B),
330 suggesting chloride extrusion along dendrites may be less effective in PV INs. However, the
331 effect of KCC2 and NKCC1 blockers on ΔE_{GABA} was not significantly different between the two
332 cell types. Thus, the KCC2 specific antagonist VU046321 produced similar reduction in the
333 somato-dendritic gradient of E_{GABA} in PV INs (-58.5 ± 3.0 %, 15 dendritic sites in 9 cells) and
334 PCs (-57.1 ± 2.7 %, 9 dendritic sites in 7 cells, $p=0.770$; Figure 4B and 5C). Further application
335 of the NKCC1 antagonist bumetanide also produced similar increase in ΔE_{GABA} in PV INs and
336 PCs (+41.5±7.2% and +45.7±8,5, respectively, as compared to VU046321 only; $p=0.67$, Figure
337 5C). This suggests NKCC1 activity may significantly contribute to transmembrane chloride

gradients in both cell types, at least upon KCC2 blockade. Altogether, these observations demonstrate chloride extrusion is more efficient along the dendrites of PCs as compared with PV INs and suggest mechanisms other than CCC function may contribute to this difference.

(Figure 4 near here)

Remarkably, although somatic chloride concentration was expected to be clamped by the internal solution of the pipette, somatic E_{GABA} was more hyperpolarized than that estimated by the Nernst equation (-41.3 mV, dashed line in Figure 5D) and more so in PV INs than PCs (53.1±1.1 *vs* 46.5±0.9 mV, n=10 and 8 cells, respectively, p=0. 003; Figure 5D). This suggests that active chloride transport i) may generate transmembrane chloride gradients that do not directly reflect the mean intracellular and extracellular concentrations and ii) is more efficient in the soma of PV INs than in PCs. Consistent with this hypothesis, somatic E_{GABA} was more depolarized upon application of VU0463271 in PV INs than in PCs (+4.9 ± 0.6 *vs* +2.8 ± 0.6 mV, n=9 and 7 cells, respectively, p=0.039; Figure 5E). Further application of bumetanide however had no significant effect on E_{GABA} in either cell type, suggesting NKCC1 does not contribute significantly to somatic transmembrane chloride gradients when intracellular chloride concentration is high (-0.43±0.4 *vs* -0.71±0.7 mV, n=8 and 7 cells, respectively, p= 0.95; Figure 5E). Altogether, our results demonstrate that KCC2 and NKCC1 are functional in PC IN s and contribute to establish steady-state transmembrane chloride gradients. The relative contribution of each transporter to somatic gradients however differ between PV INs and PCs.

(Figure 5 near here)

In order to assess both E_{GABA} and V_m while preventing perturbation of intracellular anion homeostasis, we next used gramicidin-perforated patch recordings. First, we measured V_m and tested the effect of pharmacologically blocking the excitatory drive onto CA1 PV INs and PCs, as in experiments shown in Figure 2 and 3. Whereas all PV INs were spontaneously firing at rest (frequency: 4.0±1.4 Hz, n=14 cells), application of AMPA and NMDAR blockers hyperpolarized their membrane potential by 3.5±0.6 mV (Figure 6A and 6Bb). Most PCs (12 out of 15) were also spontaneously firing but had lower firing frequency (0.23±0.1 Hz, $p<0.001$) and threshold ($p=0.006$) (Figure 6A and 6Bc). Glutamate receptor antagonists also hyperpolarized CA1 pyramidal cells, yet to a lesser extent than PV INs (0.96±0.3 mV, $p=0.001$, n= 13 cells of each type, Figure 6Bb), consistent with the latter receiving massive excitatory drive as compared with neighboring pyramidal cells (Gulyas *et al.*, 1999; Takacs *et al.*, 2012). Remarkably, these values of V_m measured in the presence of glutamate receptor antagonists were very similar to those derived from gigaseal recordings (71.6±0.6 *vs* -74.9 ± 2.0 mV (n=7) for PV INs and -74.9±1.8 vs. -74.2±0.7 mV (n=8) for PCs; Figure 3). GABAAR-mediated currents were then evoked using focal uncaging of RubiGABA, as above, and E_{GABA} was derived from current-voltage relations of somatically evoked currents (Figure 6C-D). E_{GABA} was significantly more depolarized in PV INs as compared with PCs (-64.1±2.3 *vs* -71.7±0.7 mV, $p=0.003$, n= 10 and 16 cells, respectively; Figure 6E). However, due to more depolarized V_m in PV INs (Figure 6Ba), the driving force of GABAAR-mediated currents at rest was similar in the two cell types (3.8±2.2 *vs* 1.7±1.0 mV, n=10 and 13 cells, respectively; $p=0.34$; Figure 6F). Also consistent with gigaseal recordings, E_{GABA} was slightly more depolarized than V_m both in PV INs and PCs. Application of VU0463271 depolarized somatic E_{GABA} in both cell types (by 12.5±1.6 and 16.1±1.5 mV, in PV INs (n=3) and PCs (n=8), respectively; Figure 6G) whereas further application of bumetanide only slightly

hyperpolarized E_{GABA}. This suggests that, under steady-state conditions, E_{GABA} in both PV INs and PCs is moderately depolarized as compared with V_m and predominantly influenced by the activity of KCC2, whereas NKCC1 contribution is minor. Importantly, however, although GABA may have depolarizing actions in both cells types, its effect is mostly shunting as E_{GABA} is more hyperpolarized than the action potential threshold (Figure 6H). Suppressing KCC2 activity may however be sufficient to depolarize E_{GABA} beyond this threshold, thereby promoting firing, as observed in Figure 2.

(Figure 6 near here)

Dynamic regulation of GABA signaling in CA1 parvalbumin interneurons and pyramidal cells

Repetitive activation of GABAARs has been shown in a variety of neurons to result in activity-dependent depression. This depression was attributed to intracellular chloride buildup (Thompson & Gahwiler, 1989a; Staley & Proctor, 1999; Jedlicka *et al.*, 2011) or to receptor desensitization (Thompson & Gahwiler, 1989c; Jones & Westbrook, 1995) or a combination of both. We compared the contribution of these mechanisms upon repetitive activation of GABAARs in CA1 PV INs and neighboring PCs. In order to exclude presynaptic mechanisms that may contribute to short-term, activity-dependent changes in GABA release (Thompson & Gahwiler, 1989c; Zucker & Regehr, 2002), GABAAR activation was achieved by repetitive (10 Hz), focal uncaging of RubiGABA onto the soma or dendrites of neurons recorded in gramicidin-perforated patch mode (Figure 7A). We then compared the dynamics of GABAAR-mediated currents evoked while holding cells below (-85 to -60 mV) or above (-70 to -50 mV) their reversal potential. Both in PV INs and PCs, the peak amplitude of GABAAR-mediated currents decayed with very similar kinetics during the train, independent of their polarity

(soma: τ_{inward}=0.11±0.01 vs 0.17±0.04 s^{-1}, Mann-Whitney test p=0.291; $\tau_{outward}$=0.10±0.02 vs 0.13±0.01 s^{-1}, Mann-Whitney test p=0.232; n=6 and 11 cells, respectively) and their site of initiation (soma *vs* dendrite; 0.242<p<0.695 ; Figure 7B). This observation suggests the mechanisms involved in the activity-dependent depression of GABAAR-mediated currents during a train of 10 Hz stimulation is unlikely to primarily involve changes in transmembrane ionic gradients. Consistent with this conclusion, application of the KCC2 antagonist VU0463271 had no detectable effect on the decay of outward GABAAR-mediated currents, either in PV INs ($\tau_{outward}$=0.13±0.03 vs 0.11±0.04 s^{-1}, paired t-test p=0.363; n=2 cells) or in PCs ($\tau_{outward}$=0.11±0.00 vs 0.11±0.01 s^{-1}, paired t-test p=0.848; n=4 cells ; Figure 7C). We conclude that, at least in our range of current amplitude and stimulation frequency, activity-dependent depression of GABAAR-mediated currents is largely independent of CCC function and does not reflect changes in transmembrane chloride gradients.

(Figure 7 near here)

Discussion

We have used a combination of approaches to assess and compare the polarity of GABA signaling in adult mouse CA1 hippocampal PCs and PV INs. Our results reveal that the basic mechanisms of steady-state chloride handling controlling GABA transmission are similar in both neuronal types, with a predominantly depolarizing yet inhibitory effect under resting *in vitro* conditions. PV INs and PCs, however, show different behaviors upon intracellular chloride loading, that may reflect differential distribution, regulation or efficacy of cation chloride cotransport along their somato-dendritic axis as well as electrotonic properties. Finally, we have shown that activity-dependent depression of GABAR-mediated transmission is largely independent of the polarity of the evoked currents and the activity of the transporters. This suggests this form of plasticity may not predominantly involve postsynaptic chloride loading, at least under moderate regimes of synaptic activation.

Evaluating the net effect of GABAAR activation in neurons is technically challenging as all experimental approaches may introduce some bias. Classical electrophysiological techniques may induce cell dialysis, compromise membrane integrity or underestimate Donnan potentials between pipette solution and the neuronal cytoplasm (Marty & Neher, 1995). Non-invasive approaches, such as loose-patch recordings, are then often used to assess the polarity and/or the net effect of GABAAR activation on neuronal activity (Deidda *et al.*, 2015; Lozovaya *et al.*, 2019). This approach, however, is only valid when recorded cells display spontaneous firing. As focal application of GABAAR agonists may affect the activity of neighboring neurons and subsequently modify that of the recorded neuron, we performed these recordings in the presence of glutamate receptor antagonists (Fig. 1). In the absence of

443 excitatory drive, however, most recorded neurons (either PV INs or PCs) did not exhibit
444 spontaneous firing and the effect of GABAAR activation could not be tested. These
445 experiments nevertheless showed that GABA agonists mostly inhibit spontaneously firing PV
446 INs. Cell-attached current clamp recordings provide another, minimally invasive approach to
447 evaluate the polarity of synaptic potentials as well as resting membrane potential (Perkins,
448 2006; Kirmse *et al.*, 2015). Such recordings showed that GABAAR activation mostly induces
449 membrane depolarization in both PV INs and PCs in adult mouse hippocampus, as well as in
450 PCs from immature (P3-7) hippocampus. This observation is supported by gramicidin-
451 perforated patch recordings, which revealed a depolarizing driving force for GABAAR-
452 mediated currents (Fig. 6). Although E_{GABA} was more depolarized in CA1 PV INs than in
453 neighboring PCs, the driving force of GABAAR-mediated currents was remarkably similar,
454 due to a more depolarized resting membrane potential in PV INs. Importantly, under control
455 conditions, such depolarization was not sufficient to reach action potential threshold (Fig.
456 6H), consistent with a predominantly shunting and inhibitory effect. This observation is in
457 line with earlier studies on cerebellar interneurons (Chavas & Marty, 2003), unidentified
458 hippocampal interneurons (Verheugen *et al.*, 1999; Banke & McBain, 2006) as well as
459 presumptive dentate gyrus PV INs (Sauer & Bartos, 2010).

460

461 Very few studies have explored CCC expression in cortical interneurons and data are
462 somewhat controversial, possibly due to the differential expression of distinct isoforms
463 (Uvarov *et al.*, 2007; Markkanen *et al.*, 2014). Thus, KCC2 was shown to be expressed in
464 MGE-derived interneurons earlier than in neighboring pyramidal cells during embryogenesis
465 and to control the termination of their migration (Bortone & Polleux, 2009). However, KCC2

466 expression and function in specific MGE-derived subtypes in postnatal cortex have not been
467 further explored. In the cerebellum on the contrary, KCC2 expression is very weak in early
468 postnatal presumptive baskets cells and increases postnatally (Simat *et al.*, 2007). In the
469 adult rat hippocampus, KCC2 was shown to be strongly expressed in PV-immunopositive
470 interneurons (Gulyas *et al.*, 2001), consistent with our immunohistochemical data (Fig. 1).
471 Due to the delayed expression of parvalbumin in PV INs (Solbach & Celio, 1991), we could
472 not, however, visualize CA1 PV INs in PVCre::Ai14 mice in early postnatal mice and therefore
473 could not evaluate the temporal profile of KCC2 expression and function in these cells at
474 earlier stages. In addition, the lack of a specific NKCC1 antibody for immunohistochemistry
475 precluded examination of NKCC1 expression in PV INs and PCs. Our pharmacological data,
476 however, support that both transporters are expressed and functional in both cell types in
477 PV INs and PCs in the adult mouse hippocampus. Thus, the KCC2 antagonist VU0463271 and
478 the NKCC1 antagonist bumetanide had opposing actions on i) the net effect of GABAAR
479 activation on firing (Fig 2), the efficacy of transmembrane chloride export (Fig. 5) and E_{GABA}
480 (Fig. 6) in both PV INs and PCs. Interestingly, however, although KCC2 and NKCC1 blockade
481 had similar effects on somatic E_{GABA} in PV INs and PCs in perforated-patch recordings (Fig.
482 6G), we observed significant differences when cells were loaded with high intracellular
483 chloride in whole-cell mode. Thus, the somato-dendritic gradient of E_{GABA} was more
484 pronounced in PCs than in PV INs (Fig. 5A-B) and somatic chloride extrusion was more
485 efficient in PV INs than in PCs. These differences are consistent with a differential expression
486 and/or function of KCC2 and NKCC1 along the somato-dendritic axis of the two cell types,
487 with a higher KCC2/NKCC1 function ratio in the soma of PV INs. In addition, differences in
488 the cable properties of PV IN and PC dendrites may also contribute to this difference. Thus,
489 lower membrane resistance of PV IN as compared to PC dendrites (Norenberg *et al.*, 2010)

may induce poorer space clamp of GABAAR-mediated currents evoked onto their distal dendrites. It should also be noted that, whereas the whole-cell evaluation of E_{GABA} gradients is an effective method to assess the efficacy of transmembrane chloride transport (Khirug *et al.*, 2008; Gauvain *et al.*, 2011), it may tend to overestimate steady-state KCC2/NKCC1 function ratio, as it uses high intracellular chloride concentration. This in turn is expected to inhibit the chloride-sensitive with-no-lysine (WNK) STE20 (sterile 20)-like kinases (SPAK) kinases, resulting in reduced NKCC1 and increased KCC2 function (de Los Heros *et al.*, 2014; Friedel *et al.*, 2015; Heubl *et al.*, 2017).

Activity-dependent depression of GABAAR-mediated transmission is well-documented and likely results from a combination of factors involving both pre- and postsynaptic elements (Thompson & Gahwiler, 1989a, b, c). In particular, several studies suggested repetitive activation of GABAARs may lead to postsynaptic chloride loading and a subsequent depolarization of E_{GABA} (Thompson & Gahwiler, 1989a; Kaila *et al.*, 1997; Staley & Proctor, 1999; Magloire *et al.*, 2019). However, these studies used massive chloride loading induced either by multi-quantal IPSCs or prolonged, high-frequency stimulation. Although such intense receptor activation may be relevant to specific, mostly pathological conditions (Magloire *et al.*, 2019), it may not represent the receptor activation at individual, somatic or dendritic sites. Our results from gramidicin-perforated patch recordings instead show that, upon 10 Hz focal Rubi-GABA uncaging for up to 1s, GABAAR-mediated currents decay in amplitude in both PV INs and PCs largely independent of both the direction of the ion flux and KCC2 function (Fig. 7). These results suggest that chloride accumulation during repetitive (10 Hz) activation at single somatic or dendritic sites is not sufficient to significantly affect

513 the driving force of GABAAR-mediated currents, likely owing to the rapid diffusion of
514 chloride ions inside the postsynaptic cytoplasm (Doyon *et al.*, 2011). Instead, since these
515 experiments were performed independent of synaptic stimulation, activity-dependent
516 depression of GABAAR-mediated currents likely reflected receptor desensitization (Jones &
517 Westbrook, 1996; Papke *et al.*, 2011; Gielen *et al.*, 2015). Our results demonstrate this
518 process occurs with a time constant of about 100-130 ms, consistent with the intermediate
519 component of the desensitization kinetics of recombinant $\alpha_1\beta_{1/2}\gamma_2$L receptors (Papke *et al.*,
520 2011; Brodzki *et al.*, 2016). Therefore, under physiological regimes of synaptic activity,
521 GABAAR desensitization appears as a major postsynaptic factor acting as a low-pass filter
522 with respect to GABA signaling (Jones & Westbrook, 1996).

523

524 CCC expression is altered in a variety of neurological and psychiatric conditions including
525 epilepsy (Palma *et al.*, 2006; Huberfeld *et al.*, 2007; Karlocai *et al.*, 2016; Kourdougli *et al.*,
526 2017), chronic stress (MacKenzie & Maguire, 2015), Rett syndrome (Duarte *et al.*, 2013;
527 Banerjee *et al.*, 2016; Tang *et al.*, 2016) and autism spectrum disorders (Tyzio *et al.*, 2014).
528 Impaired chloride homeostasis has been suggested to induce paradoxical excitatory GABA
529 signaling and thereby promote anomalous ensemble activities that underlie the pathology.
530 Our data also suggest that KCC2 downregulation may be sufficient to depolarize EGABA
531 above action potential threshold in PV INs (Fig. 6H). In addition, since KCC2 is involved in a
532 variety of molecular interactions with synaptic proteins (Ivakine *et al.*, 2013; Mahadevan *et*
533 *al.*, 2014), ion channels (Goutierre *et al.*, 2019) and cytoskeleton-related proteins (Li *et al.*,
534 2007; Gauvain *et al.*, 2011; Chevy *et al.*, 2015; Llano *et al.*, 2015), the loss of its expression
535 also affects several physiological properties beyond the mere control of chloride transport

and GABA signaling (Chamma *et al.*, 2012). Thus, KCC2 knockdown in cortical PCs was shown to also profoundly perturb neuronal excitability as well as network activity (Kelley *et al.*, 2018; Goutierre *et al.*, 2019). Since PV INs exert a critical control over the activity of cortical PCs (Pouille & Scanziani, 2001) and shape their rhythmic activities (Klausberger & Somogyi, 2008; Amilhon *et al.*, 2015; Gan *et al.*, 2017), altered CCC expression in these cells would be expected to profoundly perturb cortical rhythmogenesis. As most studies on CCC expression in the pathology lacked cell-subtype resolution, whether and how it is affected in PV INs remains to be fully explored and the consequences on cortical activity should then be further investigated.

References

Agetsuma M, Hamm JP, Tao K, Fujisawa S & Yuste R. (2018). Parvalbumin-Positive Interneurons Regulate Neuronal Ensembles in Visual Cortex. *Cereb Cortex* **28,** 1831-1845.

Amilhon B, Huh CY, Manseau F, Ducharme G, Nichol H, Adamantidis A & Williams S. (2015). Parvalbumin Interneurons of Hippocampus Tune Population Activity at Theta Frequency. *Neuron* **86,** 1277-1289.

Banerjee A, Rikhye RV, Breton-Provencher V, Tang X, Li C, Li K, Runyan CA, Fu Z, Jaenisch R & Sur M. (2016). Jointly reduced inhibition and excitation underlies circuit-wide changes in cortical processing in Rett syndrome. *Proceedings of the National Academy of Sciences of the United States of America*.

Banke TG & McBain CJ. (2006). GABAergic input onto CA3 hippocampal interneurons remains shunting throughout development. *The Journal of neuroscience : the official journal of the Society for Neuroscience* **26,** 11720-11725.

Bartos M, Vida I, Frotscher M, Meyer A, Monyer H, Geiger JR & Jonas P. (2002). Fast synaptic inhibition promotes synchronized gamma oscillations in hippocampal interneuron networks. *Proceedings of the National Academy of Sciences of the United States of America* **99,** 13222-13227.

Blaesse P, Airaksinen MS, Rivera C & Kaila K. (2009). Cation-chloride cotransporters and neuronal function. *Neuron* **61,** 820-838.

Bormann J, Hamill OP & Sakmann B. (1987). Mechanism of anion permeation through channels gated by glycine and gamma-aminobutyric acid in mouse cultured spinal neurones. *The Journal of physiology* **385,** 243-286.

Bortone D & Polleux F. (2009). KCC2 expression promotes the termination of cortical interneuron migration in a voltage-sensitive calcium-dependent manner. *Neuron* **62,** 53-71.

Brodzki M, Rutkowski R, Jatczak M, Kisiel M, Czyzewska MM & Mozrzymas JW. (2016). Comparison of kinetic and pharmacological profiles of recombinant alpha1gamma2L

574 and alpha1beta2gamma2L GABAA receptors - A clue to the role of intersubunit
575 interactions. *European journal of pharmacology* **784,** 81-89.

576 Buzsaki G. (2010). Neural syntax: cell assemblies, synapsembles, and readers. *Neuron* **68,**
577 362-385.

578 Chamberland S & Topolnik L. (2012). Inhibitory control of hippocampal inhibitory neurons.
579 *Frontiers in neuroscience* **6,** 165.

580 Chamma I, Chevy Q, Poncer JC & Levi S. (2012). Role of the neuronal K-Cl co-transporter
581 KCC2 in inhibitory and excitatory neurotransmission. *Frontiers in cellular*
582 *neuroscience* **6,** 5.

583 Chavas J & Marty A. (2003). Coexistence of excitatory and inhibitory GABA synapses in the
584 cerebellar interneuron network. *The Journal of neuroscience : the official journal of*
585 *the Society for Neuroscience* **23,** 2019-2031.

586 Chevy Q, Heubl M, Goutierre M, Backer S, Moutkine I, Eugene E, Bloch-Gallego E, Levi S &
587 Poncer JC. (2015). KCC2 Gates Activity-Driven AMPA Receptor Traffic through Cofilin
588 Phosphorylation. *The Journal of neuroscience : the official journal of the Society for*
589 *Neuroscience* **35,** 15772-15786.

590 de Los Heros P, Alessi DR, Gourlay R, Campbell DG, Deak M, Macartney TJ, Kahle KT & Zhang
591 J. (2014). The WNK-regulated SPAK/OSR1 kinases directly phosphorylate and inhibit
592 the K+-Cl- co-transporters. *The Biochemical journal* **458,** 559-573.

593 Deidda G, Parrini M, Naskar S, Bozarth IF, Contestabile A & Cancedda L. (2015). Reversing
594 excitatory GABAAR signaling restores synaptic plasticity and memory in a mouse
595 model of Down syndrome. *Nature medicine* **21,** 318-326.

596 Doyon N, Prescott SA, Castonguay A, Godin AG, Kroger H & De Koninck Y. (2011). Efficacy of
597 synaptic inhibition depends on multiple, dynamically interacting mechanisms
598 implicated in chloride homeostasis. *PLoS computational biology* **7,** e1002149.

599 Duarte ST, Armstrong J, Roche A, Ortez C, Perez A, O'Callaghan Mdel M, Pereira A, Sanmarti
600 F, Ormazabal A, Artuch R, Pineda M & Garcia-Cazorla A. (2013). Abnormal expression

of cerebrospinal fluid cation chloride cotransporters in patients with Rett syndrome. *PloS one* **8,** e68851.

Freund TF & Antal M. (1988). GABA-containing neurons in the septum control inhibitory interneurons in the hippocampus. *Nature* **336,** 170-173.

Friedel P, Kahle KT, Zhang J, Hertz N, Pisella LI, Buhler E, Schaller F, Duan J, Khanna AR, Bishop PN, Shokat KM & Medina I. (2015). WNK1-regulated inhibitory phosphorylation of the KCC2 cotransporter maintains the depolarizing action of GABA in immature neurons. *Sci Signal* **8,** ra65.

Gan J, Weng SM, Pernia-Andrade AJ, Csicsvari J & Jonas P. (2017). Phase-Locked Inhibition, but Not Excitation, Underlies Hippocampal Ripple Oscillations in Awake Mice In Vivo. *Neuron* **93,** 308-314.

Gao B & Fritschy JM. (1994). Selective allocation of GABAA receptors containing the alpha 1 subunit to neurochemically distinct subpopulations of rat hippocampal interneurons. *The European journal of neuroscience* **6,** 837-853.

Gauvain G, Chamma I, Chevy Q, Cabezas C, Irinopoulou T, Bodrug N, Carnaud M, Levi S & Poncer JC. (2011). The neuronal K-Cl cotransporter KCC2 influences postsynaptic AMPA receptor content and lateral diffusion in dendritic spines. *Proceedings of the National Academy of Sciences of the United States of America* **108,** 15474-15479.

Gielen M, Thomas P & Smart TG. (2015). The desensitization gate of inhibitory Cys-loop receptors. *Nature communications* **6,** 6829.

Goutierre M, Al Awabdh S, Donneger F, Francois E, Gomez-Dominguez D, Irinopoulou T, Menendez de la Prida L & Poncer JC. (2019). KCC2 Regulates Neuronal Excitability and Hippocampal Activity via Interaction with Task-3 Channels. *Cell reports* **28,** 91-103.e107.

Gulyas AI, Hajos N & Freund TF. (1996). Interneurons containing calretinin are specialized to control other interneurons in the rat hippocampus. *The Journal of neuroscience : the official journal of the Society for Neuroscience* **16,** 3397-3411.

628 Gulyas AI, Megias M, Emri Z & Freund TF. (1999). Total number and ratio of excitatory and
629 inhibitory synapses converging onto single interneurons of different types in the CA1
630 area of the rat hippocampus. *The Journal of neuroscience : the official journal of the*
631 *Society for Neuroscience* **19,** 10082-10097.

632 Gulyas AI, Sik A, Payne JA, Kaila K & Freund TF. (2001). The KCl cotransporter, KCC2, is highly
633 expressed in the vicinity of excitatory synapses in the rat hippocampus. *The European*
634 *journal of neuroscience* **13,** 2205-2217.

635 Hartig W, Brauer K & Bruckner G. (1992). Wisteria floribunda agglutinin-labelled nets
636 surround parvalbumin-containing neurons. *Neuroreport* **3,** 869-872.

637 Henze DA & Buzsaki G. (2001). Action potential threshold of hippocampal pyramidal cells in
638 vivo is increased by recent spiking activity. *Neuroscience* **105,** 121-130.

639 Heubl M, Zhang J, Pressey JC, Al Awabdh S, Renner M, Gomez-Castro F, Moutkine I, Eugène
640 E, Russeau M, Kahle KT, Poncer JC & Lévi S. (2017). GABAA receptor dependent
641 synaptic inhibition rapidly tunes KCC2 activity via the Cl−-sensitive WNK1 kinase.
642 *Nature communications* **8,** 1776.

643 Hu H, Gan J & Jonas P. (2014). Interneurons. Fast-spiking, parvalbumin(+) GABAergic
644 interneurons: from cellular design to microcircuit function. *Science* **345,** 1255263.

645 Huberfeld G, Wittner L, Clemenceau S, Baulac M, Kaila K, Miles R & Rivera C. (2007).
646 Perturbed chloride homeostasis and GABAergic signaling in human temporal lobe
647 epilepsy. *The Journal of neuroscience : the official journal of the Society for*
648 *Neuroscience* **27,** 9866-9873.

649 Ivakine EA, Acton BA, Mahadevan V, Ormond J, Tang M, Pressey JC, Huang MY, Ng D, Delpire
650 E, Salter MW, Woodin MA & McInnes RR. (2013). Neto2 is a KCC2 interacting protein
651 required for neuronal Cl- regulation in hippocampal neurons. *Proceedings of the*
652 *National Academy of Sciences of the United States of America* **110,** 3561-3566.

653 Jedlicka P, Deller T, Gutkin BS & Backus KH. (2011). Activity-dependent intracellular chloride
654 accumulation and diffusion controls GABA(A) receptor-mediated synaptic
655 transmission. *Hippocampus* **21,** 885-898.

656 Jones MV & Westbrook GL. (1995). Desensitized states prolong GABAA channel responses to
657 brief agonist pulses. *Neuron* **15,** 181-191.

658 Jones MV & Westbrook GL. (1996). The impact of receptor desensitization on fast synaptic
659 transmission. *Trends in neurosciences* **19,** 96-101.

660 Kaila K, Lamsa K, Smirnov S, Taira T & Voipio J. (1997). Long-lasting GABA-mediated
661 depolarization evoked by high-frequency stimulation in pyramidal neurons of rat
662 hippocampal slice is attributable to a network-driven, bicarbonate-dependent K+
663 transient. *The Journal of neuroscience : the official journal of the Society for*
664 *Neuroscience* **17,** 7662-7672.

665 Karlocai MR, Wittner L, Toth K, Magloczky Z, Katarova Z, Rasonyi G, Eross L, Czirjak S, Halasz
666 P, Szabo G, Payne JA, Kaila K & Freund TF. (2016). Enhanced expression of potassium-
667 chloride cotransporter KCC2 in human temporal lobe epilepsy. *Brain structure &*
668 *function* **221,** 3601-3615.

669 Kelley MR, Cardarelli RA, Smalley JL, Ollerhead TA, Andrew PM, Brandon NJ, Deeb TZ & Moss
670 SJ. (2018). Locally Reducing KCC2 Activity in the Hippocampus is Sufficient to Induce
671 Temporal Lobe Epilepsy. *EBioMedicine* **32,** 62-71.

672 Khirug S, Yamada J, Afzalov R, Voipio J, Khiroug L & Kaila K. (2008). GABAergic depolarization
673 of the axon initial segment in cortical principal neurons is caused by the Na-K-2Cl
674 cotransporter NKCC1. *The Journal of neuroscience : the official journal of the Society*
675 *for Neuroscience* **28,** 4635-4639.

676 Kim Y & Trussell LO. (2007). Ion channels generating complex spikes in cartwheel cells of the
677 dorsal cochlear nucleus. *Journal of neurophysiology* **97,** 1705-1725.

678 Kirmse K, Kummer M, Kovalchuk Y, Witte OW, Garaschuk O & Holthoff K. (2015). GABA
679 depolarizes immature neurons and inhibits network activity in the neonatal
680 neocortex in vivo. *Nature communications* **6,** 7750.

681 Klausberger T & Somogyi P. (2008). Neuronal diversity and temporal dynamics: the unity of
682 hippocampal circuit operations. *Science* **321,** 53-57.

683 Kourdougli N, Pellegrino C, Renko JM, Khirug S, Chazal G, Kukko-Lukjanov TK, Lauri SE,
684 Gaiarsa JL, Zhou L, Peret A, Castren EP, Tuominen RKP, Crepel V & Rivera CP. (2017).
685 Depolarizing GABA contributes to glutamatergic network rewiring in epilepsy. *Annals*
686 *of neurology* **81,** 251-265.

687 Li H, Khirug S, Cai C, Ludwig A, Blaesse P, Kolikova J, Afzalov R, Coleman SK, Lauri S,
688 Airaksinen MS, Keinanen K, Khiroug L, Saarma M, Kaila K & Rivera C. (2007). KCC2
689 interacts with the dendritic cytoskeleton to promote spine development. *Neuron* **56,**
690 1019-1033.

691 Llano I & Marty A. (1995). Presynaptic metabotropic glutamatergic regulation of inhibitory
692 synapses in rat cerebellar slices. *The Journal of physiology* **486 (Pt 1),** 163-176.

693 Llano O, Smirnov S, Soni S, Golubtsov A, Guillemin I, Hotulainen P, Medina I, Nothwang HG,
694 Rivera C & Ludwig A. (2015). KCC2 regulates actin dynamics in dendritic spines via
695 interaction with beta-PIX. *The Journal of cell biology* **209,** 671-686.

696 Lozovaya N, Nardou R, Tyzio R, Chiesa M, Pons-Bennaceur A, Eftekhari S, Bui TT, Billon-Grand
697 M, Rasero J, Bonifazi P, Guimond D, Gaiarsa JL, Ferrari DC & Ben-Ari Y. (2019). Early
698 alterations in a mouse model of Rett syndrome: the GABA developmental shift is
699 abolished at birth. *Scientific reports* **9,** 9276.

700 MacKenzie G & Maguire J. (2015). Chronic stress shifts the GABA reversal potential in the
701 hippocampus and increases seizure susceptibility. *Epilepsy research* **109,** 13-27.

702 Magloire V, Cornford J, Lieb A, Kullmann DM & Pavlov I. (2019). KCC2 overexpression
703 prevents the paradoxical seizure-promoting action of somatic inhibition. *Nature*
704 *communications* **10,** 1225.

705 Mahadevan V, Pressey JC, Acton BA, Uvarov P, Huang MY, Chevrier J, Puchalski A, Li CM,
706 Ivakine EA, Airaksinen MS, Delpire E, McInnes RR & Woodin MA. (2014). Kainate
707 receptors coexist in a functional complex with KCC2 and regulate chloride
708 homeostasis in hippocampal neurons. *Cell reports* **7,** 1762-1770.

709 Markkanen M, Karhunen T, Llano O, Ludwig A, Rivera C, Uvarov P & Airaksinen MS. (2014).
710 Distribution of neuronal KCC2a and KCC2b isoforms in mouse CNS. *The Journal of*
711 *comparative neurology* **522,** 1897-1914.

712 Marty A & Neher E. (1995). Tight-Seal Whole-Cell Recording. In *Single-Channel Recording*, ed.
713 Sakmann B & Neher E, pp. 31-52. Springer US, Boston, MA.

714 Mason MJ, Simpson AK, Mahaut-Smith MP & Robinson HP. (2005). The interpretation of
715 current-clamp recordings in the cell-attached patch-clamp configuration. *Biophysical*
716 *journal* **88,** 739-750.

717 Meijering E, Jacob M, Sarria JC, Steiner P, Hirling H & Unser M. (2004). Design and validation
718 of a tool for neurite tracing and analysis in fluorescence microscopy images.
719 *Cytometry Part A : the journal of the International Society for Analytical Cytology* **58,**
720 167-176.

721 Norenberg A, Hu H, Vida I, Bartos M & Jonas P. (2010). Distinct nonuniform cable properties
722 optimize rapid and efficient activation of fast-spiking GABAergic interneurons.
723 *Proceedings of the National Academy of Sciences of the United States of America* **107,**
724 894-899.

725 Palma E, Amici M, Sobrero F, Spinelli G, Di Angelantonio S, Ragozzino D, Mascia A, Scoppetta
726 C, Esposito V, Miledi R & Eusebi F. (2006). Anomalous levels of Cl- transporters in the
727 hippocampal subiculum from temporal lobe epilepsy patients make GABA excitatory.
728 *Proceedings of the National Academy of Sciences of the United States of America* **103,**
729 8465-8468.

730 Papke D, Gonzalez-Gutierrez G & Grosman C. (2011). Desensitization of neurotransmitter-
731 gated ion channels during high-frequency stimulation: a comparative study of Cys-
732 loop, AMPA and purinergic receptors. *The Journal of physiology* **589,** 1571-1585.

733 Patenaude C, Massicotte G & Lacaille JC. (2005). Cell-type specific GABA synaptic
734 transmission and activity-dependent plasticity in rat hippocampal stratum radiatum
735 interneurons. *The European journal of neuroscience* **22,** 179-188.

736 Perkins KL. (2006). Cell-attached voltage-clamp and current-clamp recording and stimulation
737 techniques in brain slices. *Journal of neuroscience methods* **154,** 1-18.

738 Pouille F & Scanziani M. (2001). Enforcement of temporal fidelity in pyramidal cells by
739 somatic feed-forward inhibition. *Science* **293,** 1159-1163.

740 Rivera C, Voipio J, Payne JA, Ruusuvuori E, Lahtinen H, Lamsa K, Pirvola U, Saarma M & Kaila
741 K. (1999). The K+/Cl- co-transporter KCC2 renders GABA hyperpolarizing during
742 neuronal maturation. *Nature* **397,** 251-255.

743 Sauer JF & Bartos M. (2010). Recruitment of early postnatal parvalbumin-positive
744 hippocampal interneurons by GABAergic excitation. *The Journal of neuroscience : the*
745 *official journal of the Society for Neuroscience* **30,** 110-115.

746 Simat M, Ambrosetti L, Lardi-Studler B & Fritschy JM. (2007). GABAergic synaptogenesis
747 marks the onset of differentiation of basket and stellate cells in mouse cerebellum.
748 *The European journal of neuroscience* **26,** 2239-2256.

749 Solbach S & Celio MR. (1991). Ontogeny of the calcium binding protein parvalbumin in the
750 rat nervous system. *Anatomy and embryology* **184,** 103-124.

751 Staley KJ & Mody I. (1992). Shunting of excitatory input to dentate gyrus granule cells by a
752 depolarizing GABAA receptor-mediated postsynaptic conductance. *Journal of*
753 *neurophysiology* **68,** 197-212.

754 Staley KJ & Proctor WR. (1999). Modulation of mammalian dendritic GABA(A) receptor
755 function by the kinetics of Cl- and HCO3- transport. *The Journal of physiology* **519 Pt**
756 **3,** 693-712.

757 Takacs VT, Klausberger T, Somogyi P, Freund TF & Gulyas AI. (2012). Extrinsic and local
758 glutamatergic inputs of the rat hippocampal CA1 area differentially innervate
759 pyramidal cells and interneurons. *Hippocampus* **22,** 1379-1391.

760 Tang X, Kim J, Zhou L, Wengert E, Zhang L, Wu Z, Carromeu C, Muotri AR, Marchetto MC,
761 Gage FH & Chen G. (2016). KCC2 rescues functional deficits in human neurons
762 derived from patients with Rett syndrome. *Proceedings of the National Academy of*
763 *Sciences of the United States of America* **113,** 751-756.

764 Thompson SM & Gahwiler BH. (1989a). Activity-dependent disinhibition. I. Repetitive
765 stimulation reduces IPSP driving force and conductance in the hippocampus in vitro.
766 *Journal of neurophysiology* **61,** 501-511.

767 Thompson SM & Gahwiler BH. (1989b). Activity-dependent disinhibition. II. Effects of
768 extracellular potassium, furosemide, and membrane potential on ECl- in hippocampal
769 CA3 neurons. *Journal of neurophysiology* **61,** 512-523.

770 Thompson SM & Gahwiler BH. (1989c). Activity-dependent disinhibition. III. Desensitization
771 and GABAB receptor-mediated presynaptic inhibition in the hippocampus in vitro.
772 *Journal of neurophysiology* **61,** 524-533.

773 Tyzio R, Nardou R, Ferrari DC, Tsintsadze T, Shahrokhi A, Eftekhari S, Khalilov I, Tsintsadze V,
774 Brouchoud C, Chazal G, Lemonnier E, Lozovaya N, Burnashev N & Ben-Ari Y. (2014).
775 Oxytocin-mediated GABA inhibition during delivery attenuates autism pathogenesis
776 in rodent offspring. *Science* **343,** 675-679.

777 Uvarov P, Ludwig A, Markkanen M, Pruunsild P, Kaila K, Delpire E, Timmusk T, Rivera C &
778 Airaksinen MS. (2007). A novel N-terminal isoform of the neuron-specific K-Cl
779 cotransporter KCC2. *The Journal of biological chemistry* **282,** 30570-30576.

780 Verheugen JA, Fricker D & Miles R. (1999). Noninvasive measurements of the membrane
781 potential and GABAergic action in hippocampal interneurons. *The Journal of*
782 *neuroscience : the official journal of the Society for Neuroscience* **19,** 2546-2555.

783 Zucker RS & Regehr WG. (2002). Short-term synaptic plasticity. *Annu Rev Physiol* **64,** 355-
784 405.

785

786

Acknowledgements

We thank X. Marques for expert assistance with confocal imaging, which was performed at the "Photonic Imaging and Image Analysis Platform" of the Institut du Fer à Moulin. We also thank Peter Blaesse for critical reading of the manuscript.

Competing interests

The authors declare no conflict of interest.

Author contributions

Y.O. and J.C.P. conceived and designed the research. Y.O. performed all electrophysiological recordings and data analysis with help of E.J.S. who also maintained the mouse colony. F.D. performed immunohistochemistry, confocal imaging and analysis. Y.O and J.C.P. prepared the figures and wrote the paper. All authors approved the final version of the manuscript and agree to be accountable for all aspects of the work in ensuring that questions related to the accuracy or integrity of any part of the work are appropriately investigated and resolved. All persons designated as authors qualify for authorship, and all those who qualify for authorship are listed.

807 **Funding**

808 This work was supported by the Institut National de la Santé et de la Recherche Médicale,
809 Sorbonne Université, LabEx Bio-Psy through the *Investissements d'Avenir* program managed
810 by Agence Nationale de La Recherche under reference ANR-11-IDEX-0004-02 (postdoctoral
811 fellowship to YO), Fondation pour la Recherche Médicale (grant DEQ20140329539 to JCP),
812 Fédération pour la Recherche sur le Cerveau and Fondation Française pour la Recherche sur
813 l'Epilespie (grants to JCP) as well as ERANET-Neuron (ACRoBAT project, funded by Agence
814 Nationale pour la Recherche to JCP). FD is the recipient of a doctoral fellowship from
815 Sorbonne Université. The Poncer lab is affiliated with the Paris School of Neuroscience (ENP)
816 and the Bio-Psy Laboratory of excellence.

817

Figures and legends

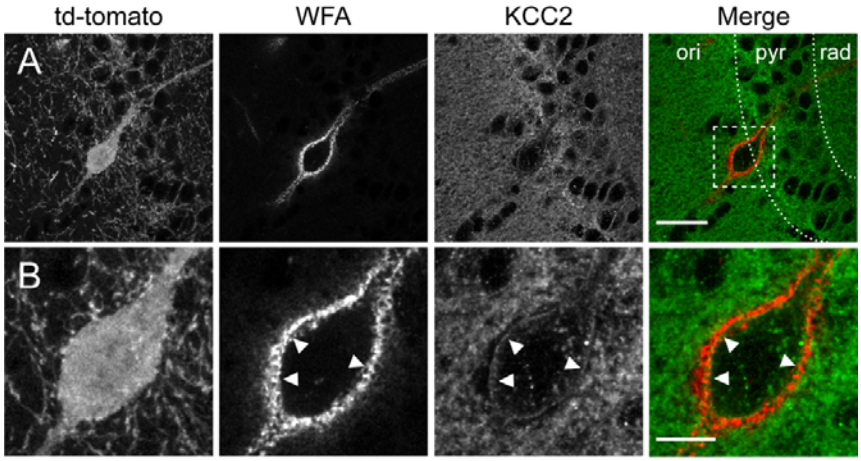

Figure 1. KCC2 labeling of hippocampal CA1 parvalbumin interneurons.

A, Representative micrograph (maximum projection of 10 confocal sections over 2.6 µm) of area CA1 of an adult *Pvalb*$^{tm1(cre)Arbr/J}$*::Ai14* mouse hippocampal section immunostained for KCC2 (green) and WFA lectin (red), showing td-tomato expression in a PV IN surrounded by WFA staining on the soma and proximal dendrites. Scale, 30 µm. B, Magnified region boxed in A, showing KCC2 immunostaining in td-tomato expressing PV IN lies just underneath the perineuronal net stained with WFA (arrowheads). Scale, 10 µm.

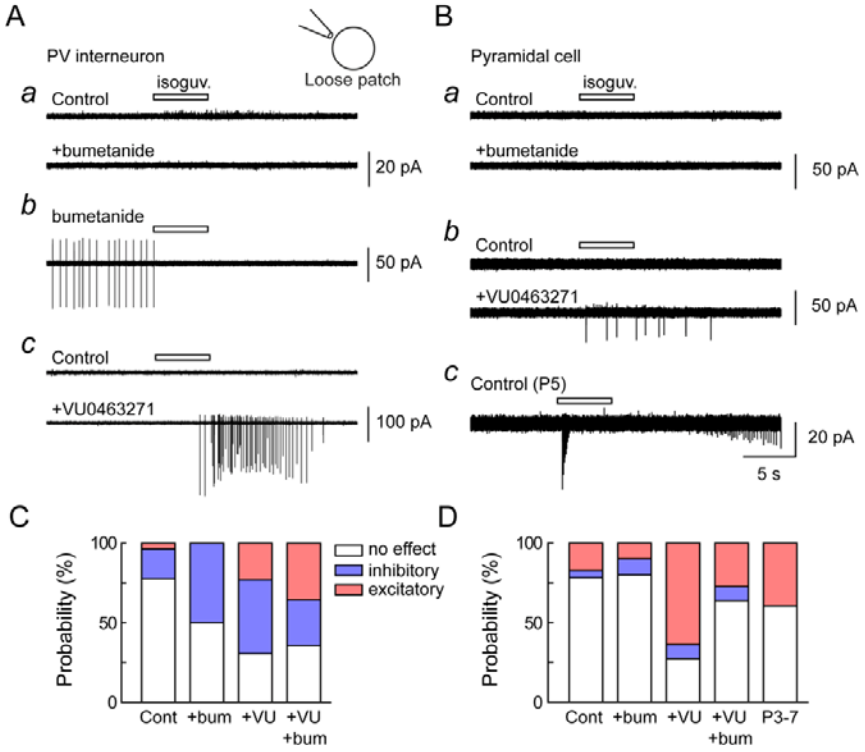

828

829 **Figure 2. Excitatory and inhibitory actions of GABAA receptor activation in CA1**

830 **parvalbumin interneurons and pyramidal cells.**

831 A *a*, Representative sections of recordings in loose patch mode of a CA1 PV IN upon brief,

832 focal somatic application of isoguvacine (100 µM, white bar), before and during application

833 of the NKCC1 antagonist bumetanide (10 µM). *b*, same as in *a* in another PV IN during

834 bumetanide application. *c*, same as in *a* and *b*, before and during application of the KCC2

835 antagonist VU0463271 (10 µM). B *a* and *b*, recordings as in A *a* and *c* from CA1 PCs in P30-

836 P40 mice. *c*, recording showing the effect of somatic isoguvacine application on a CA1 PC

837 from a P5 mouse. C, summary graph showing the proportions of each type response

838 (excitatory, inhibitory or none) recorded upon isoguvacine application in PV INs. D, Same as

839 C for recordings from PCs.

840

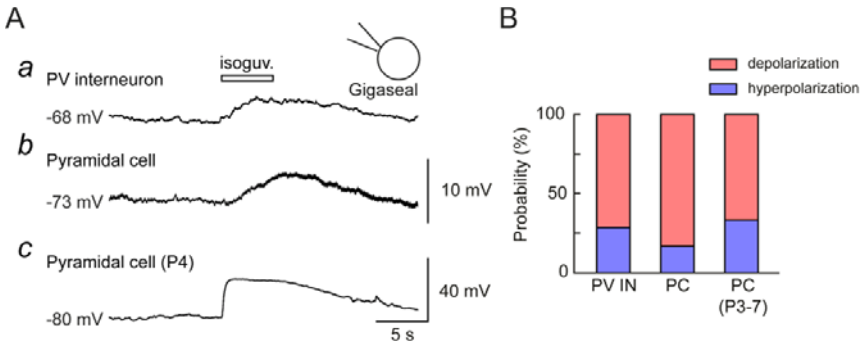

Figure 3. Polarity of GABAAR-mediated potentials in CA1 parvalbumin interneurons and pyramidal cells.

A, Representative sections of recordings in gigaseal patch mode of a CA1 PV IN from a P46 mouse (*a*) and a PC from a P33 (*b*) or P4 (*c*) mouse upon brief, focal somatic application of isoguvacine (100 µM, white bar). B, summary graph showing the proportions of each type of response (depolarizing, hyperpolarizing) recorded upon isoguvacine application in each cell type.

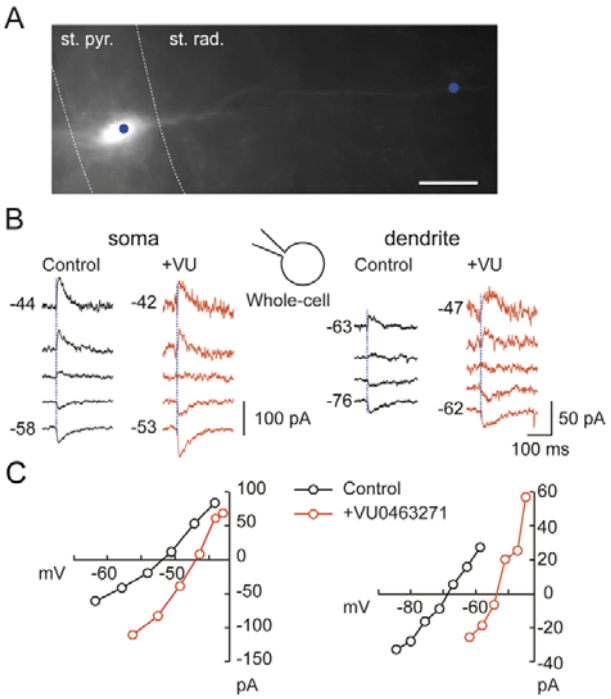

Figure 4. Contribution of KCC2 to transmembrane chloride extrusion in a CA1 parvalbumin interneuron.

A, Fluorescence micrograph of a CA1 PV IN from a P37 mouse hippocampal slice, recorded in whole-cell mode and filled with Alex594. The blue spots represent the position and size of the laser beam used for focal RubiGABA photolysis. Scale, 20 µm. B, Currents evoked at varying potentials by focal somatic (left) or dendritic (right) photolysis of RubiGABA in the cell shown in A, before (black) and during (red) application of VU0463271 (10 µM). Numbers of the right represent holding potentials corrected for liquid junction potential and voltage drop across the pipette resistance. C, Current-voltage relations from recordings shown in B showing the different reversal potentials of RubiGABA-evoked currents in the soma vs. dendrites and their depolarizing shift upon KCC2 blockade.

872

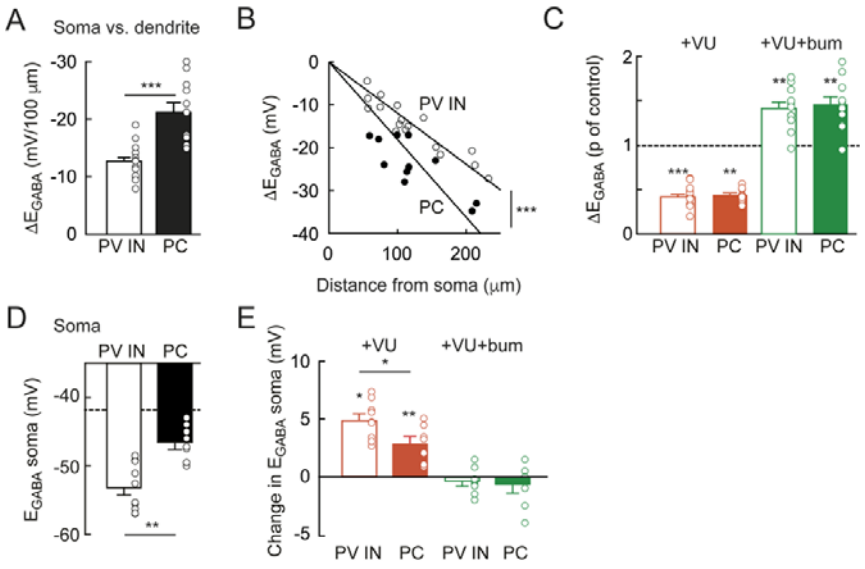

873

874 **Figure 5. Compared contribution of KCC2 and NKCC1 to somato-dendritic chloride**

875 **gradients in CA1 parvalbumin interneuron and pyramidal cells.**

876 A, Summary graph showing E_{GABA} somatodendritic gradient (ΔE_{GABA}) between soma and

877 dendrites normalized by the distance from soma to dendritic photolysis locations. PV IN:

878 n=17 dendritic sites in 9 cells. PC: n=11 dendritic sites in 8 cells. *** Mann Whitney test

879 p<0.001. B, somatodendritic E_{GABA} gradient plotted against the distance from soma to

880 dendritic photolysis locations with superimposed linear regression, showing steeper relation

881 in PCs compared with PV INs. Same data as in A, *** Multiple regression test p<0.001. C,

882 Change in ΔE_{GABA} upon sequential KCC2 (red) and KCC2+NKCC1 blockade (green) by

883 VU0463271 and bumetanide, respectively. The values are normalized to those of the

884 preceding condition (control for VU0463271, VU0463271 for VU0463271+bumetanide). **

885 and *** Wilcoxon signed-rank test p<0.01 and 0.001, respectively. No significant difference

886 was observed in PC vs PV INs. Same recordings as in A and B. D, Reversal potential (E_{GABA}) of

887 currents evoked by somatic RubiGABA uncaging in PV INs and PCs. Same data as in A-C.

888 Dashed line: estimated E_{Cl} based on Nernst equation. ** Mann Whitney test $p<0.01$. E,
889 Change in somatic E_{GABA} upon sequential KCC2 (red) and KCC2+NKCC1 blockade (green) by
890 VU0463271 and bumetanide, respectively. The values are normalized to those of the
891 preceding condition (control for VU0463271, VU0463271 for VU0463271+bumetanide).
892 VU0463271 depolarized E_{GABA} more in PV INs than in PCs. However, further addition of
893 bumetanide had no significant effect. * and ** Wilcoxon rank signed-rank test $p<0.05$ and
894 0.01, respectively. * for PV INs vs PCs, Mann Whitney test $p<0.05$.

895

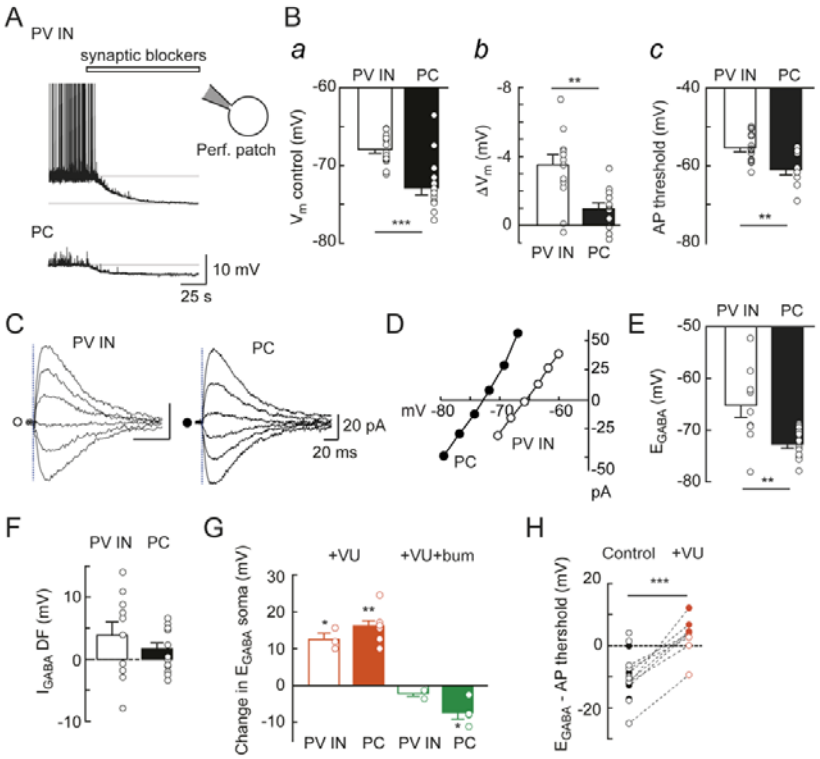

Figure 6. Compared reversal potential and driving force of GABA currents in CA1 parvalbumin interneurons and pyramidal cells.

A, Representative current clamp recordings from a CA1 PV IN (top) and PC (bottom) in gramicidin-perforated patch mode, showing the effect of synaptic receptor antagonists (APV, NBQX and CGP55845) and TTX (white bar) on holding potential. Note that the PV IN but not the PC shows spontaneous firing prior to application of the blockers. B, *a*, resting membrane potential measured in 15 CA1 PV INs and 15 PCs prior to application of synaptic blockers. ***, Mann Whitney test p<0.001. *b*, change in membrane potential (ΔV_m) upon application of synaptic blockers in the same cells as in *a*. **, Mann Whitney test p<0.01. *c*, Action potential threshold measured in spontaneously firing PV INs (n=15) and PCs (n=9). **, Mann Withney test p<0.01. C, Currents evoked at varying potentials by focal somatic photolysis of RubiGABA in a PV IN (left) and a PC (right). The dotted line represents the

timing of photolysis. D, corresponding current/voltage relation for the recordings shown in C. Open circles, PV IN. Filled circles, PC. E, Summary graphs showing the reversal potential of somatically evoked GABAAR-mediated currents in 10 CA1 PV INs and 16 PCs. **, Mann Whitney test $p<0.01$. F, estimated driving force of somatic GABAAR-mediated currents computed by subtracting Vm from E_{GABA}, showing GABAARs have slightly depolarizing actions in both PV INs and PCs. G, summary graph showing the change in somatic E_{GABA} upon sequential KCC2 (red) and KCC2+NKCC1 blockade (green) by VU0463271 and bumetanide, respectively. The values are normalized to those of the preceding condition (control for VU0463271, VU0463271 for VU0463271+bumetanide). Addition of bumetanide after VU0463271 had no significant effect on somatic E_{GABA} in either PV INs (n=3) or PCs (n=4). *, paired t-test, $p<0.05$; **, Wilcoxon signed rank test, $p<0.01$. H, Difference between E_{GABA} and firing threshold for PV INs (open circles) and PCs (filled circles), before (black) and during (red) application of VU0463271. Dotted lines represent paired data used for statistical comparison (all cells pooled). ***, Paired t-test, $p<0.001$.

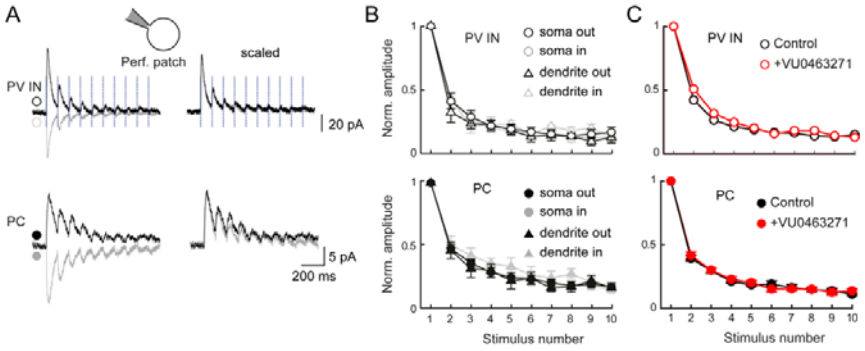

Figure 7. Dynamics of GABAAR-mediated currents in CA1 parvalbumin interneurons and pyramidal cells.

A, Representative recordings of currents evoked by 10 Hz somatic photolysis of RubiGABA in a CA1 PV IN and a PC recorded in gramicidin-perforated patch mode and held at potentials above (black) or below (grey) E_{GABA} (PV IN: -60 and -80 mV; PC: -60 and -77 mV). B, Summary graphs showing peak current amplitudes normalized to the peak amplitude of the first current, during a train of RubiGABA photolysis on the soma (circles) or dendrites (triangles) of PV INs (soma: n=6, dendrites: n=3, open symbols) and PCs (soma: n=11, dendrites: n=4, filled symbols). C, Same as in B showing the lack of effect of VU0463271 (10 µM, red symbols) on the decay of the peak amplitude of GABAAR-mediated currents during a 10 Hz somatic RubiGABA photolysis (PV INs, n=2; PCs, n=4).